PAGEOPH, Vol. 125, No. 4 (1987)

0033-4553/87/040629-28$1.50+0.20/0

A Two Degree-of-Freedom Earthquake Model with Static/Dynamic Friction

JEFFREY NUSSBAUM [1] and ANDY RUINA [2]

Abstract—Can a simple multi-block-spring model with total symmetry make interesting predictions for fault behaviour? Our model consists of a symmetric, slowly driven, two degree-of-freedom block-spring system with static/dynamic friction. The simple friction law and slow driving rate allow the state of this fourth order system to be described between slip events by a single variable, the difference in the stretch of the driving springs. This stretch difference measures the locked-in stress and is closely related to fault stress inhomogeneity.

In general, *smoothing* is not observed. A spatially homogeneous stress state is found to almost always be unstable, in that the system tends toward an inhomogeneous state after many slip events. The system evolves either to a cycle that alternates between two types of earthquakes, or to a cycle with repeating but identical asymmetric earthquakes. One type of alternating earthquake solution is structurally unstable, which implies a great sensitivity to model perturbations.

For this simple model, spatial asymmetry necessarily occurs, despite the symmetry in the model, thus suggesting that spatial structure in seismicity patterns may be a consequence of earthquake dynamics, not just fault heterogeneity.

Key words: Earthquake, friction, stick-slip, symmetry.

Introduction

One approach to the understanding of seismicity patterns and earthquakes is the construction of deterministic models. These models are used with the hope of simulating seismic patterns, and observing such features as a reasonable frequency-magnitude relationship, stable and unstable slip, preseismic slip, aftershocks, and stress deficit roughening. Since understanding is now at a fairly primitive stage, insight may be gained by examining both the predictions and limitations of simple models. A crude class of such models uses blocks, springs, and friction.

Many have investigated the possible role of the friction law on instabilities and pre- and post-seismic slip by using a single block model, including BYERLEE (1970, 1978), DIETERICH (1980, 1981), RICE and TSE (1986), GU *et al.* (1984), CAO and AKI

[1] Currently at General Electric Company, Lynn, MA 01910, USA.

[2] Department of Theoretical and Applied Mechanics, Cornell University, Ithaca, NY 1480, USA.

(1986), BLANPIED and TULLIS (1986), WEEKS and TULLIS (1985), RUINA (1983), and NUR (1978). Though such models aid in the understanding of frictional instabilities, they are limited by their inability to model spatial variations. To address the spatial aspect of seismicity patterns, BURRIDGE and KNOPOFF (1967) studied (experimentally and numerically) a one-dimensional chain of blocks connected by springs. Others followed up using similar models, but different friction laws, elastic properties, initial states, and loading conditions.

One frequent observation in numerical simulations of multi-block models is the presence of 'smoothing,' a term which has had several meanings. ANDREWS (1975, 1978) used smoothing to mean the tendency (over many slip events) for the state of stress along the fault to move toward a more uniform spatial distribution (*stress smoothing*). However, Cao and Aki (1986) defined the term to indicate the transition from events in which few or small regions on the fault slip, to events where many or large regions on the fault slip, until eventually every event involves slip along the entire fault (*event smoothing*). These similar definitions have subtle differences, for it is possible for a heterogeneous stress distribution to still lead to nearly simultaneous slip of many regions and hence large earthquakes. Stress smoothing leads to event smoothing, but event smoothing does not necessarily imply stress smoothing. The appearance of smoothing is thought to be an unrealistic prediction of an earthquake model, because it seems inconsistent with real seismic patterns. For example, the entire San Andreas fault does not slip in every earthquake. Rather, a complicated spatial structure seems to persist over the centuries.

The simulations and experiments of BURRIDGE and KNOPOFF (1967) do not indicate either stress or event smoothing as previously defined. Their work shows evidence of cycles of smoothing, then roughening. Large events were preceded and followed by numerous smaller events. ANDREWS (1975, 1978) found stress smoothing using a numerical two-dimensional elastic plate model, static/dynamic friction, and uniform fault strength. In the three initial conditions he tried, the 'self energy', a measure of fault stress heterogeneity, decreased during a simulated earthquake event. He claimed that in order to predict seismicity patterns, a model must include inhomogeneous material properties, branching and bending of the fault zone, migration of pore fluids, or a more complicated friction law. COHEN (1977) also studied a multiple block model. He introduced spatial variations in elastic and frictional parameters and did not observe smoothing of either kind. NUR (1978) and ISRAEL and NUR (1979) concluded that inhomogeneous properties are essential to the maintenance of spatial structure in seismic patterns. DIETERICH (1972) also varied material properties in space, using elastic and viscoelastic models and static/dynamic or time dependent friction. He found no smoothing. Viscoelasticity and time dependent static friction also allowed him to simulate aftershocks. In their spring block model with static/dynamic friction, Cao and Aki (1986) describe event smoothing, independent of heterogeneity in frictional strength. They claim that the coupling ratio C/L (the coupling stiffness C divided by the driving spring stiffness L) must be sufficiently low

(as in COHEN (1977) and DIETERICH (1972)) in order to preclude even smoothing. Cao and Aki proceeded to use a more complex friction law with spatially inhomogeneous properties in order to mimic certain aspects of seismicity patterns.

The research succeeding BURRIDGE and KNOPOFF (1967) attempted to simulate seismic features by choosing elaborate spatially-varying models for friction and fault strength. What we would like to address is: can a simple model produce certain kinds of complex behavior? HOROWITZ and RUINA (1986) found complex spatial patterns with a homogeneous two-dimensional elastic fault model, and a rate and state dependent friction law. Based on these results (and in opposition to some of the papers cited above) we suspect that some of the complexity of earthquakes is due to the appropriate governing equations having complicated solutions, even in the absence of inhomogeneous material properties and complicated friction laws. To address this question in a simple way, we simulated a strike-slip fault using a two-block mass-spring model with static/dynamic friction. Our emphasis is on the patterns of events after many slip cycles have occurred over long periods of time.

After describing the model, we will show that the configuration of our two-block system is characterized by a single variable, the difference in stretch of the driving springs at the end of an event. The subsequent values of this stretch difference are then used to describe the long-term dynamics of the system. We look at trajectories in configuration space, utilizing a *failure locus*, and display the system configuration as a function of its previous configuration with a *one-dimensional iteration map*. The one-dimensional map is used to describe the evolution and stability of the system.

The Model

The two-block model, which will be further simplified below, is shown in Figure 1. Two masses are connected by a linear spring with spring constant k_c and driven by a slowly moving support. The support is coupled to the masses by springs of stiffness k_1 and k_2. Between the blocks and their supports are the friction forces F_1 and F_2 (in general not constant). Here m_1 and m_2 represent the masses, and y_1 and y_2 are the position coordinates (spring stretches) for each mass, referred to the driver. The driver, which is assumed to move at a constant rate, is meant to represent inexorable tectonic processes; the masses are two regions near a fault surface; the springs k_1 and k_2 are connections between the remote loading and the fault; the coupling spring k_c is the interconnection between fault regions. The springs, k_1, k_2 and k_c represent appropriate stiffnesses for the axial and shear deformation in strike-slip or thrust faulting. Roughly, k_1 and k_2 are shear springs for strike-slip faulting (the case schematically represented in Figures 1 and 2), the axial springs for thrust faulting; while k_c is an axial spring for strike-slip faulting and a shear spring for thrust faulting.

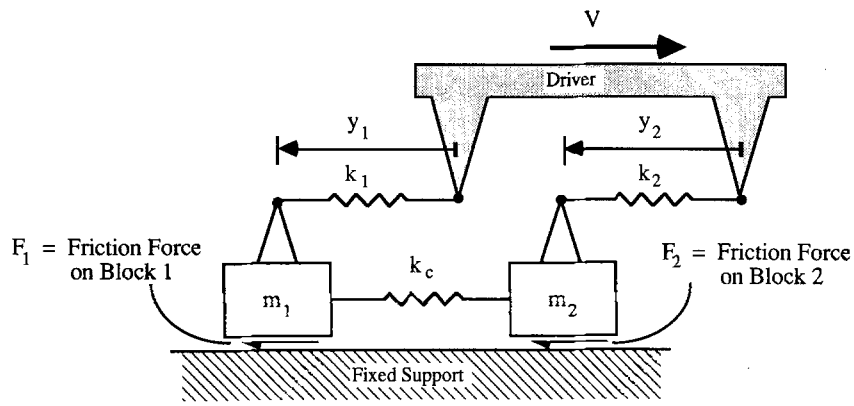

Figure 1
Schematic of a Discrete (Block-Spring) Earthquake Model. Two massive blocks are connected by springs and slowly loaded. Friction inhibits block motion.

Newton's second law leads to the following equations of motion:

$$\begin{aligned} m_1\ddot{y}_1 + (k_1 + k_c)y_1 - k_c y_2 &= F_1 \\ m_2\ddot{y}_2 + (k_2 + k_c)y_2 - k_c y_1 &= F_2 \end{aligned} \tag{1}$$

For plausible friction laws (the functional form of the dependence of F_i on the slip history $[Vt - y_i(t)]$ (with $i = 1, 2$)), equations (1) represent at least a fourth-order nonlinear system of ordinary differential equations. We make the following further simplifications:

1) The driver is assumed to move slowly, so slowly that it may be considered stationary during any block motion (as in BURRIDGE and KNOPOFF (1967)). Thus driver motion loads the system but $V = 0$ is used in all dynamical calculations.
2) Complete spatial uniformity is assumed. By moving from a general to a symmetric model, the problem may be examined in greater depth. Also, an interesting question can be addressed, namely whether a symmetric model produces asymmetric solutions. Accordingly, we set $m_1 = m_2 = m$, and $k_1 = k_2 = k$ as indicated in Figure 2. The coupling spring constant is defined in terms of k: $k_c = \alpha k$. For this two block system, this reflection symmetry is also equivalent to translation symmetry and a periodic boundary condition. The friction forces also are assumed to have no spatial dependence.
3) The friction is static/dynamic. It is characterized by F_s, the static friction force (at impending slip), and F_d, the dynamic friction force (during slip). Each is assumed to be constant. Static/dynamic friction (together with slow driver motion) leads to stick-slip. Thus there will be a long loading period (during which no blocks slide), then a sliding period, then another loading period,

and so forth. Later some results will be generalized to other friction laws, such as an added linear rate dependency (which might be used to simulate elastodynamic radiation, as suggested by BURRIDGE and KNOPOFF (1967)).

4) Slip occurs in only one direction (block velocities are never positive during slip). Reverse slip is forbidden. It is easily shown that reverse slip never occurs in a single block model if $F_s/F_d < 3$. We feel the restriction is reasonable for a multiple block-spring model, since physically realistic values of F_s/F_d are probably not much larger than unity.

The equations of motion are simplified by a change of variables based on the above assumptions. Time is rescaled: $t = \tau\sqrt{(k/m)}$, where τ is original time and t is dimensionless time. A dimensionless spring stretch s_i is defined by scaling and offsetting y_i: $(i = 1, 2)$

$$y_i = s_i \frac{(F_s - F_d)}{k} + \frac{F_d}{k} \quad \text{or inversely} \quad s_i = \frac{y_i k}{F_s - F_d} - \frac{F_d}{F_s - F_d}. \tag{2}$$

Thus we obtain the system shown in Figure 2, which is fully equivalent to the system in Figure 1 when the assumption of symmetry is made and static/dynamic friction (with no reverse slip) is used. The masses, driving springs, and static friction force are now all unity. The coupling spring constant (equivalent to the coupling ratio C/L in CAO and AKI (1986)) is α, and the dynamic friction force is zero.

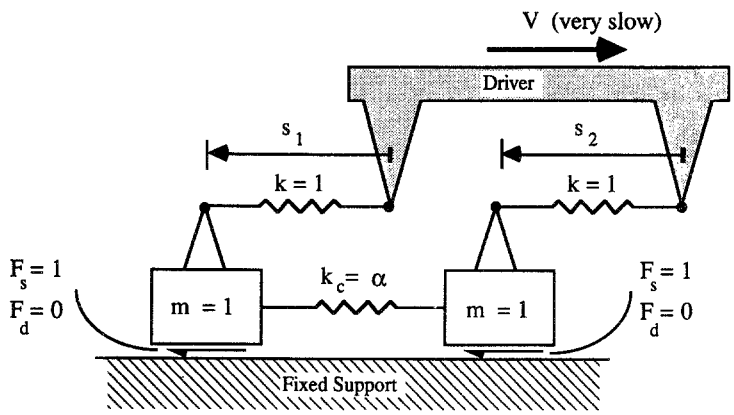

Figure 2

Scaled Schematic Model. After scaling of variables and assumptions of spatial uniformity, the only system parameter is the coupling ratio α.

A balance of forces leads to conditions on s_1 and s_2 for impeding slip:

$$\begin{aligned} (1 + \alpha)s_1 - \alpha s_2 &= 1 \quad \text{for block 1 to slip} \\ (1 + \alpha)s_2 - \alpha s_1 &= 1 \quad \text{for block 2 to slip.} \end{aligned} \tag{3}$$

For any n-block system, the conditions for slip onset can be viewed on a *failure locus* shown in n-dimensional configuration space $(s_1, s_2 \ldots s_n)$. Slip does not occur until the failure locus is reached, that is to say some $f(s_1, s_2, \ldots s_n)$ reaches a critical value. An arbitrary two-dimensional failure locus in (s_1, s_2) coordinate space is shown schematically in Figure 3. The failure locus we use, equation (3), shown in Figure 4. Slip begins when the trajectory in configuration space (as influenced by the remote loading) reaches the failure locus.

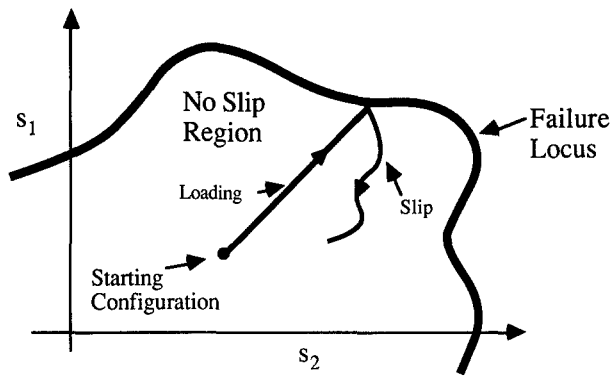

Figure 3

Schematic Graph of a Two-dimensional Failure Locus. The dark line is the failure locus, representing all (s_1, s_2) pairs for impending slip using an arbitrary model. No slip occurs until the the trajectory reaches the failure locus.

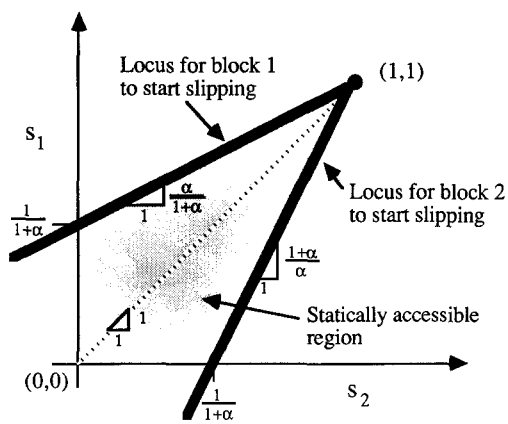

Figure 4

Actual Two-block Failure Locus. The static friction force is overcome when a trajectory $(s_1(t), s_2(t))$ reaches the failure locus. The shape of the locus depends only on the coupling ratio α. It tends to a unit square as $\alpha \to 0$, and approaches a pair of 45° lines as $\alpha \to \infty$.

We have the following equations of motion during slip.

$$\begin{aligned} \ddot{s}_1 + (1 + \alpha)\, s_1 - \alpha\, s_2 = 0 \quad &\text{while block 1 slides } (\dot{s}_1 < 0) \\ &\text{(otherwise } \dot{s}_1 = 0) \\ \ddot{s}_2 + (1 + \alpha)\, s_2 - \alpha\, s_1 = 0 \quad &\text{while block 2 slides } (\dot{s}_2 < 0) \\ &\text{(otherwise } \dot{s}_2 = 0) \end{aligned} \tag{4}$$

The only parameter in our model (see Figure 2 or equations (3), (4)) is the coupling ratio α. That and the initial positions fully determine all subsequent motion. Our fourth-order nonlinear system has been reduced to a homogeneous linear system (4). The nonlinear effects of friction only appear in the conditions for the onset and termination of slip (equation (3) and assumption (4)).

Numerical Solution

Although the general solution of (4) is easily obtained, finding when a block stops ($\dot{s}_1 = 0$ or $\dot{s}_2 = 0$) involves solving a transcendental equation. Rather than solve this transcendental equation, a numerical method was used to integrate the equations of motion when both blocks were moving. The scheme was a second-order Runge-Kutta, with a fixed step size of $1/(25\ \omega_2)$ where ω_2 is the higher characteristic frequency of (4), to be mentioned later. The size was occasionally adjusted manually to check for numerical convergence. Values of the coupling ratio α between 0.1 and 100.0 were investigated, with emphasis placed on values of α less than 10.0. For every value of α, at least 200 initial conditions were used.

Because this model contains static/dynamic friction, the program had to check to see if the blocks were stopped so the correct friction force could be applied. To prevent reverse slip, the program looked for a sign change in velocity. As soon as one was observed, the block was considered stopped, and was not allowed to resume sliding until it again satisfied its failure criterion (3).

Block Motion

The system is started from rest in some initial configuration (s_1, s_2), with slip not yet impending and $s_1 \neq s_2$. (The case where $s_1 \equiv s_2$ is special, leading to both blocks starting at once.. This will be mentioned later.) The driver slowly moves, and the springs become more stretched. After sufficient stretch, one block starts to move and the driver is considered motionless. The moving block will eventually come to rest, but while it slides it increases the load on the other block, and it may trigger the other block to start sliding. One or both blocks move, and finally both come to rest. This motion could also include multiple slips, in which each block starts and stops several times before the system comes to rest. For future reference, we define an *event* to be the cycle from the system starting at rest until it next comes to rest. After the event, loading is resumed by means of slow driver motion.

Characterization of System Configuration by the Stretch Difference

The motion of this fourth order system may be characterized for some purposes by the sequence of values of a single scalar variable, the stretch difference $(s_1 - s_2)$. When the system loads (without slip), s_1 and s_2 increase at the same rate until the failure locus is reached, as shown in line A-B in Figures 5 and 6. Thus $(s_1 - s_2)$ does not change until a block (in this case block 1) starts to slip (point B in Figures 5 and 6). At point B, the state of the system is completely known: the trajectory is at the failure locus, and the stretch difference $(s_2 - s_2)$ is the same as it was at the beginning of loading (this is the end of the preceding event, at which time the difference $(s_1 - s_2)$ was known from previous dynamics). Together, the failure locus and $(s_1 - s_2)$ determine (s_1, s_2). Since both blocks' slip velocities are zero, the full state of the system is determined by $(s_1 - s_2)$ at impending slip.

In some sense, $(s_1 - s_2)$ at impending slip represents a Poincaré section (a cross section of the phase space — see GUCKENHEIMER and HOLMES (1984), for example). Though a trajectory of the system state,

$$(s_1(t), s_2(t), \dot{s}_1(t), \dot{s}_2(t)),$$

lies in a four-dimensional phase space, the Poincaré section is not three-dimensional but one-dimensional since the trajectory at this section is known to lie on the plane

$$\dot{s}_1 = \dot{s}_2 = V.$$

The evolution of the system from event to event can be described by the sequence of values taken by the stretch difference. This sequence is characterized by a one-dimensional map, the nature of which is discussed in a later section.

The stretch difference $(s_1 - s_2)$ is a useful variable to follow since it is a measure of locked-in stress (self-stress, or the part of the frictional stress which does not change during loading) and fault stress inhomogeneity. The quantity $(s_1 - s_2)^2$ is proportional to the 'self energy' discussed in ANDREWS (1978).

Types of Events

Several types of events have been observed. *One-block* events are simplest, involving only a single block moving before the system comes to rest. *Two-block* events have both blocks sliding, perhaps several times each. If both blocks undergo identical simultaneous motion, the event is called *homogeneous.*

One-block Events

Figure 5 shows a trajectory plotted on the (s_1, s_2) plane for a one-block event (B-C). The system loads slowly along a 45° line (A-B and C-D), with both springs stretching at equal rates. When one of the two failure loci is reached, the respective block starts to slip. Suppose the system starts out with $s_1 > s_2$ as shown in Figure 5 at A. Then it is clear that the block-1 locus will be reached before the block-2 locus, and block 1 will slip first, starting at point B.

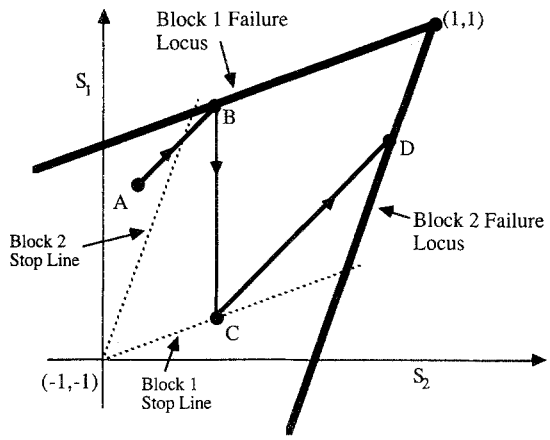

Figure 5

Trajectory in Configuration Space for a One-block event. The system loads until the trajectory reaches the failure locus. Dashed lines parallel to the failure loci represents stop lines. The trajectory for a one-block event ends at a stop line. Loading is shown as (A-B) and (C-D). Slip is shown as (B-C).

If only one block moves during an event, it slides a fixed distance (COHEN (1977)) independent of its starting point. This follows say, from the first of the failure conditions (3) (neither block is moving, block 1 will slip first) being applied as an initial condition to the first equation (4) (block 1 slips, s_2 is held constant) and then finding s_1 when block 1 stops moving. The net change in s_1 is independent of $(s_1 - s_2)$. The calculation is carried out in equations (6) and (7) below. The result can also be physically reasoned as follows: A single block will slide when the total spring force it feels reaches F_s (which has been scaled to unity here). Because the springs are linear, the net force the block feels at initiation of slip (and during slip) is independent of locked-in stress. Thus the block motion and sliding distance are also independent of locked-in stress in any one-block event. Such an event results in a friction force drop of $2(F_s - F_d)$.

Using this fixed sliding distance result, two stop lines can be defined (the dotted lines in Figure 5), parallel to each failure locus. In configuration space, a lone sliding block will move in a straight horizontal or vertical line (B-C in Figure 5) until its

trajectory reaches the proper stop line. The stop lines have meaning only for single-block events. If only block 1 moves, the only s_1 changes, and slip is a vertical line downward from the failure locus (s_2 is constant). Similarly, if only block 2 moves, the trajectory is a horizontal (leftward) line. Slip cycles that do not involve simultaneous motion of both blocks appear as horizontal and vertical slip lines, and 45° loading lines in configuration space. The systems loads, a block slips, then the system loads again (A-B-C-D in Figure 5). The location of the failure locus and stop lines entirely define the sequence of one-block slip events.

In general, the slip distance in a one-block event is independent of the initial stretch difference $(s_1 - s_2)$ when using any friction law with the following functional form:

$$\text{friction} = f(\delta, \dot{\delta})$$

where δ is the slip distance in the current event and $\dot{\delta}$ is the slip rate. This implies a straight stop line parallel to the failure locus. Static/dynamic friction is a special case of such a friction law. Also included are linear viscous damping and simple slip weakening (friction is a decreasing function of δ).

The preceding argument (for a straight stop line parallel to the failure locus) is carried out in detail for the friction law used in our simulations, as follows. In a one-block event, the motion is simple harmonic during slip. With a mass of unity and an effective spring constant of $(1 + \alpha)$, this motion has a frequency of:

$$\omega = \sqrt{1 + \alpha} \tag{5}$$

The equations of motion (4), with initial conditions of zero velocity, $(s_1 - s_2)_{init}$ given, and s_1 and s_2 on the block 1 failure locus, have solution:

$$\begin{aligned} s_1 &= \frac{1}{1 + \alpha}\left[\cos[\sqrt{1 + \alpha}t] + \alpha\right] - \alpha(s_1 - s_2)_{init} \\ s_2 &= \text{constant} = 1 - (1 + \alpha)(s_1 - s_2)_{init} \end{aligned} \tag{6}$$

Here $(s_1 - s_2)_{init}$ refers to the stretch difference during loading.

To find s_{1stop} (the equation of the stop line), equation (6) is used to set the velocity of block 1 to zero. We obtain:

$$s_{1stop} = \frac{\alpha - 1}{1 + \alpha} - \alpha(s_1 - s_2)_{init} \tag{7}$$

The slip distance in a one-block event is $[s_{1init} - s_{1stop}] = 2/(1 + \alpha)$ (from (3), (6) and (7), say). Here s_{1init} is the value of s_1 at impending slip. The force drop is 2

units, obtained from an energy balance, or by using this slip distance and the effective spring constant of $(1 + \alpha)$.

Two-block Events

If a second block should start to slip while the first was moving, a different motion would result, an example of which is shown as B-B′-C′-C in Figure 6. This is the case if the system configuration reaches the other failure locus (at B′) before hitting the first stop line. The trajectory is initially straight (B-B′), but then the second block starts to move when its failure locus is reached at B′. The ensuing motion is a combination of both normal modes, and appears as a curved path on the (s_1, s_2) plane. The characteristic frequencies for the normal modes are:

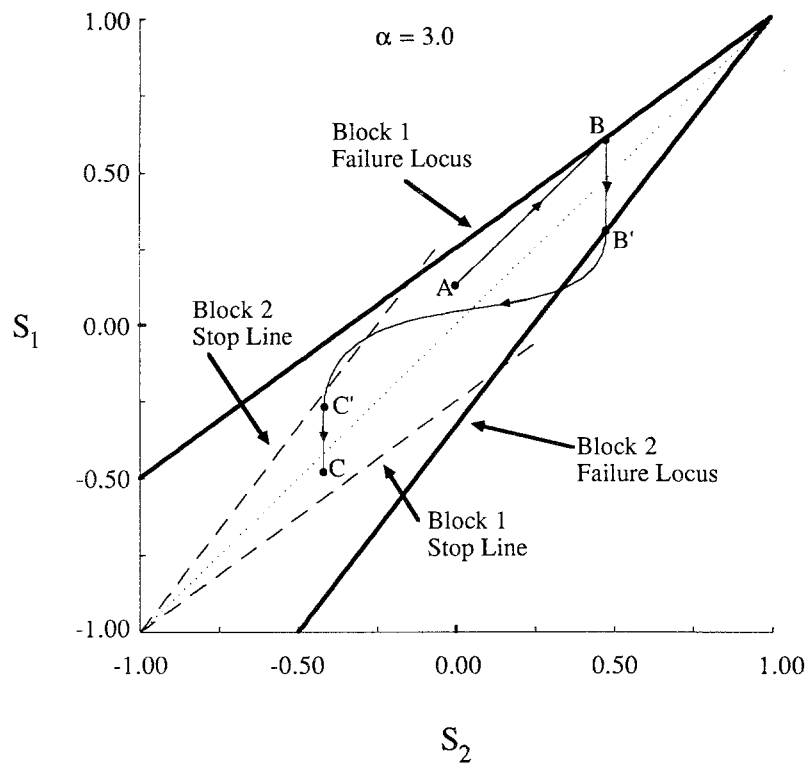

Figure 6

A Two-Block Event in Configuration Space. The loading part of the trajectory has unit slope (A-B). Only a single block slips (B-B′) until the second failure locus is reached at B′. Both blocks slide until C′ is reached, when block 2 stops. Block 1 stops at C. The trajectory A-B-B′-C′-C constitutes a type of two-block event. The stop lines (which are not relevant in this event) are also shown. The event shown is not a part of a periodic orbit.

$$\begin{aligned} \omega_1 &= 1 \\ \omega_2 &= \sqrt{1 + 2\alpha}. \end{aligned} \tag{8}$$

(In general, the system completes only about half a (slower) cycle of oscillation.) Note that ω_2 gets large for large α. Thus we have multiple time scales, and the system of differential equations is 'stiff' if the coupling spring is much stiffer than the drive springs ($\alpha \gg 1$).

Two-block events occur if s_1 and s_2 are sufficiently close together at failure. In other words, the event starts close to the apex of the failure locus, as in B-B′ in Figure 6 (but not as in B-C in Figure 5). A geometric construction shows the following condition for two-block events.

$$|s_1 - s_2|_{init} < \frac{2\alpha}{(1 + \alpha)(1 + 2\alpha)}. \tag{9}$$

When the trajectory hits the second failure locus (at B′ in Figure 6) and s_2 begins to change, the velocity of block 1 (from (3) and (6)) is:

$$\dot{s}_1 = -\frac{1}{\omega}\sqrt{1 - \frac{1}{\alpha^2}[(1 - \omega^2(s_1 - s_2)_{init})\omega_2^2 - \omega^2]^2}. \tag{10}$$

Now both blocks will be moving, and we have a superposition of the four normal mode solutions to equation (4):

$$\begin{aligned} s_1 &= C_1 \cos(t) + C_2 \sin(t) + C_3 \cos(\omega_2 t) + C_4 \sin(\omega_2 t) \\ s_2 &= C_1 \cos(t) + C_2 \sin(t) - C_3 \cos(\omega_2 t) - C_4 \sin(\omega_2 t). \end{aligned} \tag{11}$$

The four constants C_i are determined by applying (11) to the following:

s_1, s_2 are on the failure locus (as given in (7) and the second of equations (6))

$$\begin{aligned} s_1 &= \frac{\alpha - 1}{1 + \alpha} - \alpha(s_1 - s_2)_{init} \\ s_2 &= s_{2init} \end{aligned}$$

and

$$\begin{aligned} &\dot{s}_1 \text{ is given by (10)} \\ &\dot{s}_2 = 0. \end{aligned}$$

Of course, the C_i's determined in this way are valid only during the first part of motion when both blocks are moving. After one block stops (at C′ in Figure 6, say), the equations of motion (4) must be solved again, using the current system state as initial conditions.

Homogeneous Events

Finally there is the case of $(s_1 - s_2)_{init} \equiv 0$. Such an initial condition starts on the 45° line $y = x$ of the failure locus and hits the intersection (apex) of the two failure loci. Both blocks start to slide at the same time. Their motions will be identical and $(s_1 - s_2)$ will remain zero throughout the slip and all subsequent events. Thus the event is called homogeneous. This corresponds to rigid body motion of the fault, and is the motion that would be seen in a one-block system or a completely smoothed system. However, any small deviation from $(s_1 - s_2)_{init} \equiv 0$ results in a qualitatively different motion, as will be discussed.

Multiple Events

For high values of α, the failure loci are quite narrow, and two-block events can involve more than one start and stop motion for each block. Such a multislip event is shown in a configuration space plot (Figure 7) for $\alpha = 10.0$. Possible implications of this more complicated motion and high α are mentioned later.

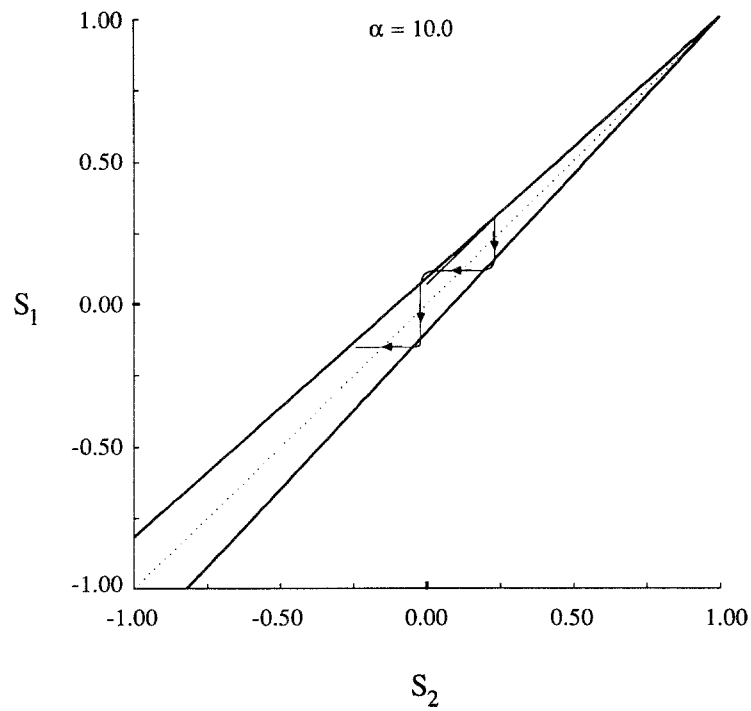

Figure 7

Multiple-slip Event in Configuration Space. This trajectory shows blocks 1 and 2 each slipping twice in one event. This is not a periodic orbit. Multiple slips can occur for certain initial conditions if the coupling ratio α is relatively high. Figure 14 shows a different representation of a high α simulation.

Sequences of Events

After an event, the system slowly reloads, one of the blocks reaches its failure locus, and another event begins. In this model, a sequence of events crudely represents long-term seismicity patterns.

All of our simulations settle to one of several well-defined sequences of events: Either identical events occur repeatedly, or two different events repeat alternately. In the language defined below, all of these eventual sequences correspond to orbits with periods of either 1 or 2.

The sequence of events is described by the sequence of values of the stretch difference $(s_1 - s_2)$ as discussed previously. The sequences for all possible initial conditions are characterized by the function relating $(s_1 - s_2)$ before one event to $(s_1 - s_2)$ before the previous event. This function is an iteration map.

A Review of Iteration Mappings

The brief discussion of iteration mappings given here will help in the interpretation of plots that appear later. A more thorough treatment can be found in DEVANEY (1986).

An iteration mapping is a function of one variable $f(x)$ used to determine a sequence of values x_n. Thus x_0 leads to $x_1 = f(x_0)$ which leads to $x_2 = f(x_1) = f(f(x_0))$ and so forth. More compactly, x_n, the nth iterate of $f(x)$ is written as $f^n(x)$ or $f_n(x)$. Iteration maps are typically graphed in the form $f(x)$ versus x, equivalent to a plot of $f^{n+1}(x)$ versus $f^n(x)$ or x_{n+1} versus x_n. For our study, x_n is the stretch difference just before event n, $(s_1 - s_2)_n$.

For a given map f: A *fixed point* is defined to be any x such that $f(x) = x$. It appears on the iteration map graph as an intersection of the curve $f(x)$ with the 45° line $y = x$. A point x and its iterates comprise a *periodic orbit of period n* if $f^n(x) = x$. A fixed point can correspond to a *limit cycle*, which is a periodic orbit of period 1 that is unique in its own neighborhood.

The slope of a (smooth) function f (the iteration map) determines the stability of its fixed points. A fixed point *repels* (is unstable) if the slope at that point has magnitude greater than 1, and *attracts* (is stable) if the slope magnitude is less than 1. If the slope equals ± 1, higher derivatives are necessary to determine stability at that point. An attracting fixed point x_0 has the property that for x sufficiently close to x_0 (inside the *region of attraction*), $f^{n+1}(x)$ is closer to x_0 than $f^n(x)$. A repelling point has an analogous property. A fixed point with slope of ± 1 is called *nonhyperbolic*; otherwise it is called *hyperbolic*. Nonhyperbolic fixed points have the property of being *structurally unstable*, meaning a small change in the model can result in a qualitative change in the sequence of events.

Figures 8 show sample numerically-generated iteration maps $(s_1 - s_2)_{n+1}$ versus $(s_1 - s_2)_n$, for $\alpha = 1.0$, $\alpha = 1.35$ and $\alpha = 2.0$. The computer simulation generates

many points by solving the equations of motion for 200 or more initial conditions. These points have been connected by smooth curves.

A function f can be iterated graphically as follows: from any point on the curve, find the next iterate by moving horizontally to the 45° line, then vertically to the curve. (This does not yield an actual trajectory, but only the next point on the graph.) In all three figures, the origin (0, 0) is seen to have a slope of magnitude greater than 1, so it is unstable (a repelling point), and iterations diverge (as shown by graphical iteration in Figures 8a and 8c). However, Figure 8b shows convergence to one of two stable (attracting) fixed points (points A).

In general, an *nth*-iteration mapping is necessary to detect period-n orbits and classify their stability. However, the antisymmetry of the maps presented here (which follows from the symmetry of our model) makes some period-2 orbits easy to detect. Any intersection of the curve with the $-45°$ line $y = -x$ will represent a period-2 orbit. The approach to this orbit is also shown as a spiral out from near the origin in Figure 8c. Another period-2 orbit is shown as the larger square in Figure 8c. The approach to this orbit is not shown. It is not a limit cycle, since all points on the map curve in the bracketed part of Region I also represent period-2 orbits. A limit cycle of period 2 is represented as the inner square in Figure 8c, where iteration maps a point A to the corresponding point in the diagonally opposite quadrant, and then back to the starting point, and so on.

For purposes of discussion, we label three regions on the iteration map curve. For larger values of α, new discontinuities (which are not shown in Figures 8, but do appear in Figure 14) appear on the map between Regions I and III. They are due to changes between different types of events.

Period-1 Orbits: Homogeneous Events

A period-1 orbit is found at the origin (0, 0) of all of the iteration maps. It is clear that if the system starts out with $s_1 \equiv s_2$, then it will end up that way. However, the iteration maps show that this fixed point is usually not stable, because except for special cases, the magnitude of the slope at the origin is greater than 1. Thus regardless of how small $(s_1 - s_2)$ starts, it will diverge from the origin. A sequence of simulations started at various points near $(s_1 - s_2) = 0$ yielded the iteration map near the origin. Each numerically-obtained iteration map plotted on log-log axes showed a power low relationship near the origin:

$$(s_1 - s_2)_{n+1} = A(s_1 - s_2)_n^b. \tag{12}$$

Here A and b are constant for given α. The exponent b was observed to always lie between zero and one, equaling unity only or the cases of $\alpha = \alpha_n$, with α_n defined as:

$$\alpha_n = \frac{n^2 - 1}{2} (n = 2, 3 \ldots). \tag{13}$$

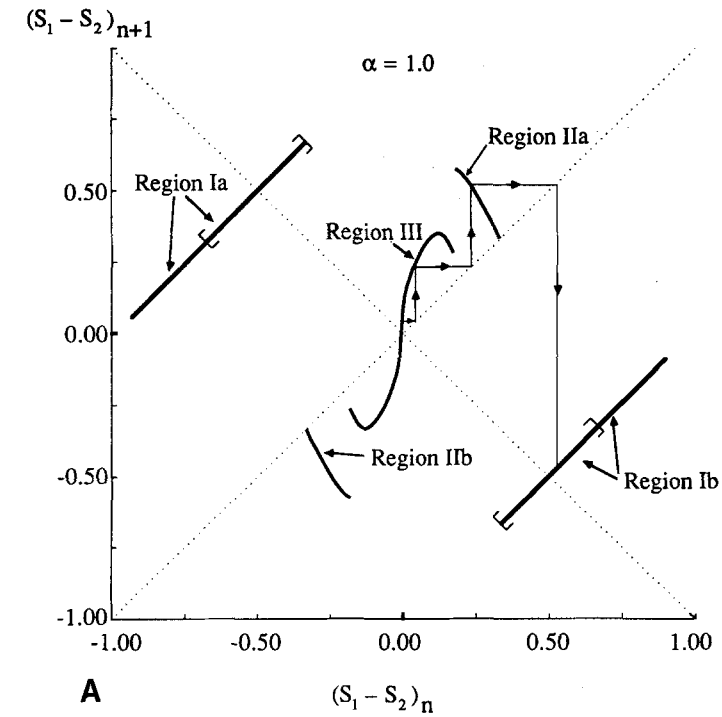
$(S_1 - S_2)_{n+1}$
α = 1.0
Region Ia
Region IIa
Region III
Region IIb
Region Ib
0.50
0.00
-0.50
-1.00
-1.00
-0.50
0.00
0.50
1.00
A
$(S_1 - S_2)_n$

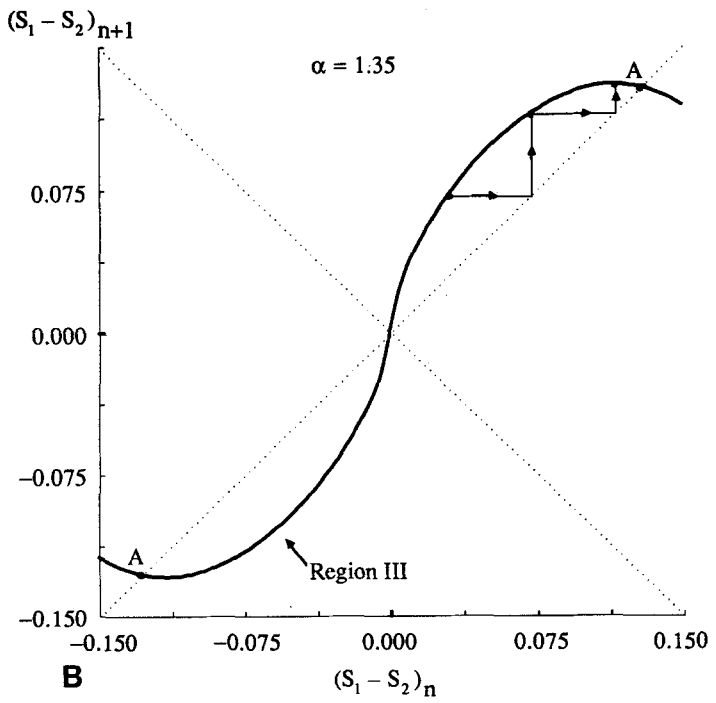
$(S_1 - S_2)_{n+1}$
α = 1.35
A
A
Region III
0.075
0.000
−0.075
−0.150
−0.150
−0.075
0.000
0.075
0.150
B
$(S_1 - S_2)_n$

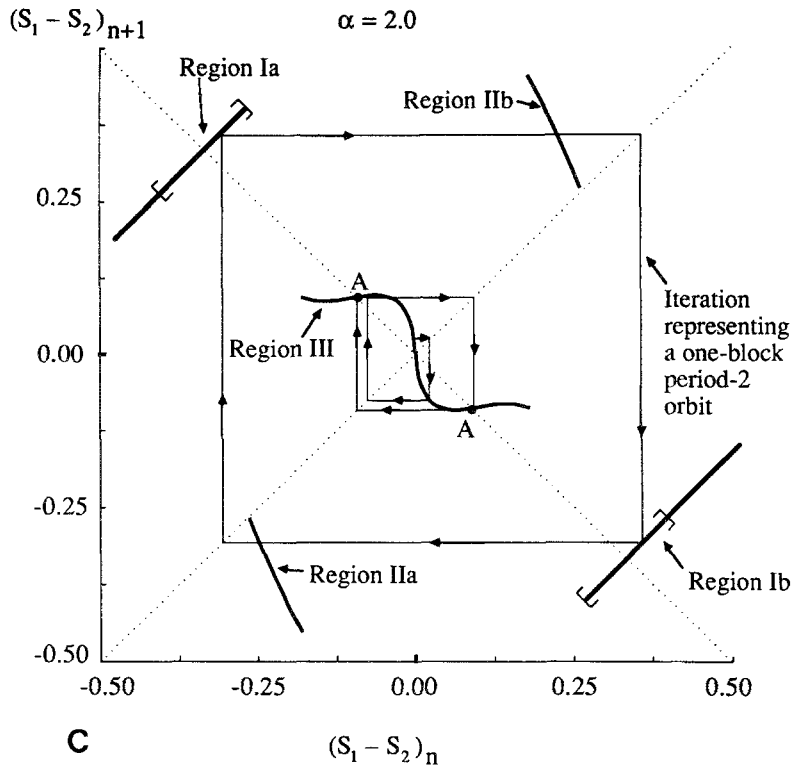

Figures 8a,b,c

Iteration Map Graphs. System configuration $(s_1 - s_2)$ after an event versus configuration before the event. These curves describe the evolution of the system. Regions on the curve are labeled for discussion. Intersections of the solid curve with the 45° line $y = x$ represent period-1 orbits. Intersections of the solid curve with the $-45°$ line $y = -x$ represent period-2 orbits, due to symmetry. A fixed point (period-1 orbit) attracts if its slope has magnitude less than 1, repels if the magnitude is greater than 1, and is neutrally stable if the slope equals ± 1. Given $(s_1 - s_2)_n$ find $(s_1 - s_2)_{n+1}$ graphically by moving horizontally to the 45° line, then vertically to the solid curve as indicated.

8A. **Iteration Map Graph for α = 1.0.** Graphical iteration shows a point near the origin diverging from the fixed point and approaching the periodic part of Region I. The brackets in Region I bound its periodic portion. (This periodic oribit is not shown in the figure, but a smiliar orbit is shown in Figure 8c).

8B. **Iteration Map Graph for α = 1.35.** This close up of the center of the iteration map shows two fixed points, where the curve intersects the 45° line at points A. Graphical iteration shows the approach to a fixed point, which is similar to the trajectories shown in Figure 10. All maps follow a power law close to the origin.

8C. **Iteration Map Graph for α = 2.0.** The iteration map graph intersects the $-45°$ line at points A, resulting in a two-block period 2 orbit. This orbit is shown in configuration space in Figure 12. Graphical iteration is shown starting near the origin and entering this limit cycle. One-block period-2 orbits are also found for all points in the bracketed part of region I. The square indicates one such orbit period-2 orbit. (A similar orbit is shown in configuration space in Figure 11).

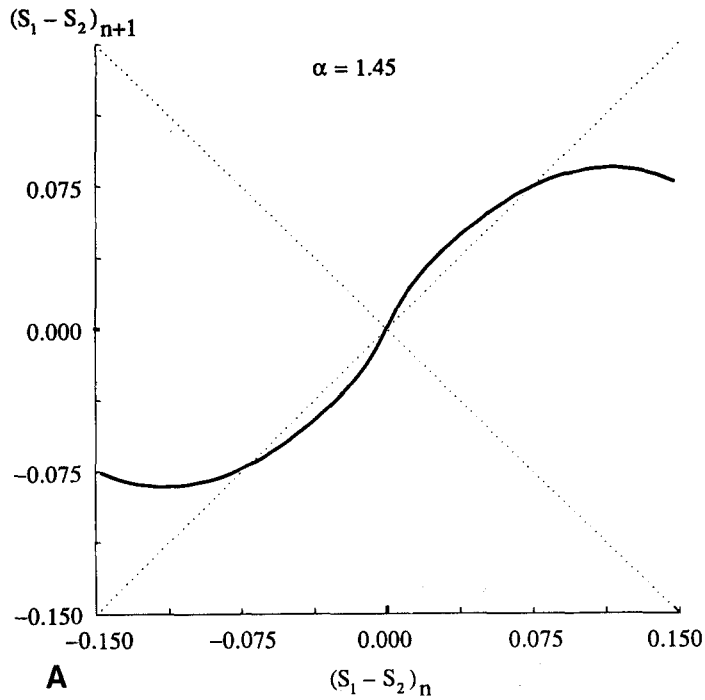
$(S_1 - S_2)_{n+1}$
α = 1.45
0.075
0.000
−0.075
−0.150
−0.150
−0.075
0.000
0.075
0.150
A
$(S_1 - S_2)_n$

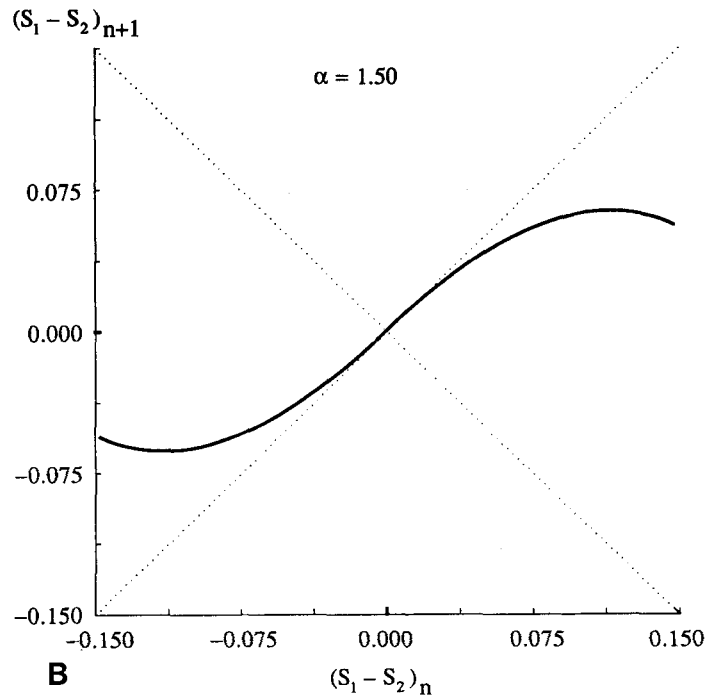
$(S_1 - S_2)_{n+1}$
α = 1.50
0.075
0.000
−0.075
−0.150
−0.150
−0.075
0.000
0.075
0.150
B
$(S_1 - S_2)_n$

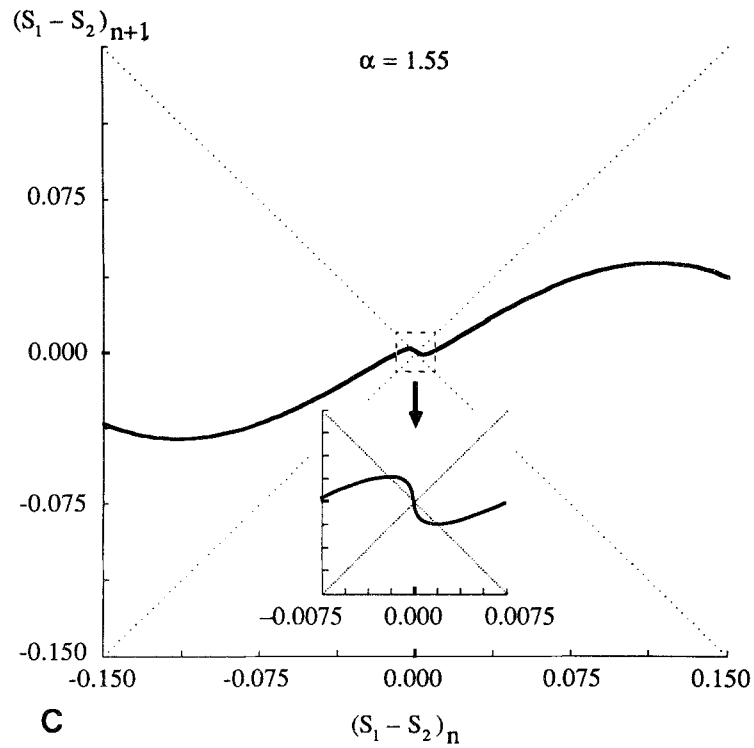

Figure 9

Change in the Iteration Map as α Passes Through α_n. The slope of the iteration map graph changes sign, starting near the origin and gradually spreading to all of Region III (defined in Figure 8) as α gets further from α_n. In (a), α = 1.45 and the map is continuous, with a weak singularity at the origin. In (b), α = 1.5 and the map is linear near the origin. When α = 1.55 (c), the iteration map has changed sign close to the origin (see insert), where the slope has magnitude greater than one (still infinite *at* the origin). Further from the origin, the map has not changed much from the α_n case shown in Figure 9b.

$\alpha = \alpha_n$ corresponds to the ratio of natural frequencies ω_1/ω_2 in (8) having integer values. Except for these special values of α, the power law exponent b is less than one, meaning the map is singular at the origin, and the slope there is positive or negative infinity. Since the degree of instability of a fixed point is governed by the magnitude of its slope, the origin is infinitely unstable. However, as α approaches α_n, the strength of this singularity decreases, until finally when $\alpha = \alpha_n$, the singularity disappears and the origin is barely stable. These asymptotic results could possibly be derived by analytic means but we have not done so.

When the natural frequencies have integer ratios and the power law exponent is unity, the iteration mapping is linear near the origin. As the coupling ratio passes through any α_n, an interesting change appears in the graph of the iteration map. In addition to the strength of the singularity changing, the slope of Region III changes sign near the origin. An example is given in Figures 9 for $\alpha_n = 1.5$. The region near

the origin is shown in detail. Figure 9a ($\alpha = 1.45$) shows the positive slope and the effects of the weak singularity (the region of infinite slope is too small to be clearly seen.). The intersections with the line $y = x$ represent period-1 oribits. When α is increased to 1.5 (Figure 9b), the origin is no longer singular. Finally as α passes α_n (Figure 9c, $\alpha = 1.55$), the central-most region has slope opposite in sign to the maps for α slightly smaller than α_n. As α gets larger, this central-most region grows in size. The iteration map shown in Figure 9c has intersections with the line $y = -x$, representing period-2 orbits. Each time α passes through α_n, the iteration map changes between intersecting the $y = x$ line and the $y = -x$ line, meaning the type of oribit switches between period-1 and period-2.

Another interesting phenomena is associated with α passing through α_n. For α slightly greater than α_n, the iteration map graph has x-axis intersections in addition to the usual crossing at (0, 0). These values of $(s_1 - s_2)$ map into the fixed point at the origin, resulting in homogeneous slip. However, as previously stated, the origin is singular and therefore unstable.

When $\alpha = \alpha_n$, (Figure 9b) the map is asymptotically linear at the origin. The origin is a weakly attracting fixed point, leading to homogeneous slip (for some initial configurations). These are the only observed instances of complete stress smoothing.

Period-1 Orbits: Asymmetric Global Events

Another type of fixed point is shown on the iteration map graph of Figure 8b as points A. Here the slope of the mapping has magnitude less than unity at the fixed points, so the period-1 orbit is stable for this value of α. The orbits are nonalternating asymmetric global events: global in that both blocks move during the event; asymmetric in that the two blocks do not start or stop at the same times; nonalternating in that they are period-1, with the same block starting first in each event. The block that starts moving first will stop moving last. However, both blocks slip the same distance during the event. Such an event occurs only when α is in certain ranges. Figure 8b shows graphical iteration of the approach to the fixed point. A trajectory corresponding to this convergence is plotted in configuration space in Figure 10.

Period-2 Orbits: One-block Events

Several types of period-2 oribits have been discovered. The first is a family of one-block period-2 orbits, which is found in the bracketed part of Region I, shown in Figures 8a and 8c. The periodic sequence involves one-block events that alternate between blocks (loading, block 1 slips then stops; loading; block 2 slips then stops, etc.). The nonperiodic events in Region I start outside the range marked with

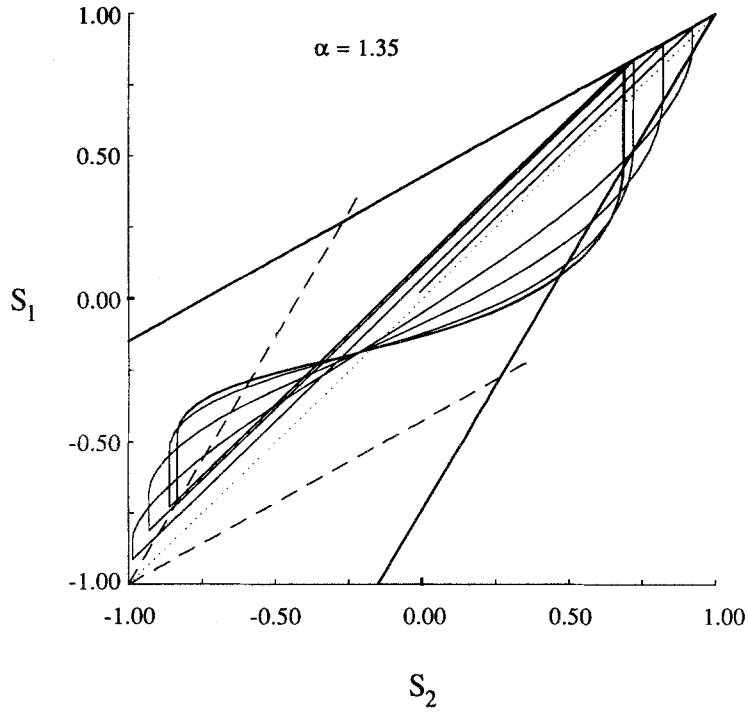

Figure 10

Period-1 Limit Cycle. This trajectory is approaching a nonalternating asymmetric period-1 limit cycle, shown in configuration space. An initial configuration with $(s_1 - s_2)$ small is diverging from that state (through subsequent events) and converging to a period-1 limit cycle. The iteration map corresponding to this coupling ratio is shown in Figure 8b.

brackets, thus representing initial states of extreme heterogeneity, which is partly smoothed in subsequent events. (These nonperiodic motions are still one-block events.) For the periodic part of Region I, a point with coordinates (x, y) maps to its reflected mirror image $(-x, -y)$ after one event, and back to itself (x, y) after two events. This limit cycle appears as a closed 'bow tie' in configuration space, which is shown in Figure 11 (D-E-F-G). For the point in Region I on the $-45°$ line, the pair of one-block events would appear as a symmetric 'bow tie' in configuration space. The time between events differs for different points in the periodic part of Region I. In particular, this time is equal for a symmetric 'bow tie', and asymptotically approaches zero where Region I is closest to Region II (and the 'bow tie' distorts to a triangle). The existence of this family of period-2 oribits can be justified graphically in the configuration plane, by noting that the failure locus is symmetric with respect to the 45° line (meaning the failure loci and the stop lines form a rhombus, as shown in Figure 5).

The periodic part of Region I is stable in some sense, in that all points that enter remain. Region I has unit slope due to the constant stress drop $F_s - F_d$ (or constant

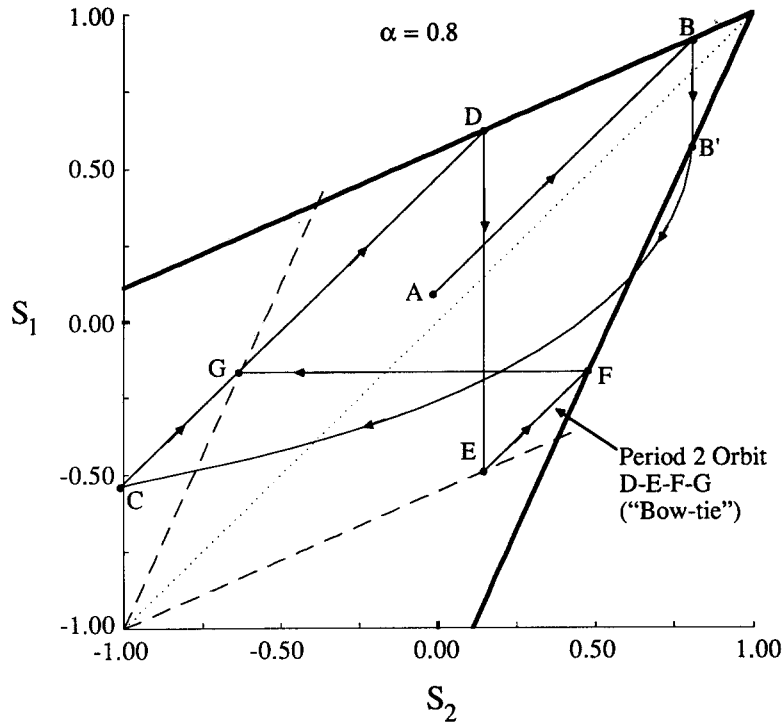

Figure 11
One-block Orbit of Period 2. The initial configuration (point A) has led to a two-block event (B-B′-C), then to a one-block 'bow tie' orbit of period 2 (D-E-F-G). (See the outer square of Figure 8c.)

slip distance) for a one-block event. That and the antisymmetry of the mapping imply that the second iterate f^2 of the periodic part of Region I has a family of unit-slope fixed points. Thus the periodic part of Region I is not structually stable (since all points are nonhyperbolic when twice iterated).

Some changes in the friction law might change the shape of Region I, and thus eliminate the presence of the family of period-2 orbits in Region I. But, as previously mentioned, the stress drop will also be constant if the model uses rate and/or slip displacement dependent friction. For such friction laws, period-2 orbits, unit slope and the structural instability of Region I are maintained.

Period-2 Orbits: Asymmetric Global Events

The second class of period-2 orbits are represented by points A in Figure 8c. They are alternating asymmetric global events: alternating in that they are period-2; asymmetric in that the blocks do not start at the same time; global in that both

blocks move in the event. The block that starts moving first will stop moving last, and slips a greater distance than the other block. The configuration space trajectory of this limit cycle is shown in Figure 12. For $\alpha = 2.0$, the region of attraction is all of Region III. In particular, a point arbitrarily close to the origin diverges and is attracted into this limit cycle. Like the period-1 motion being approached in Figure 10, these period-2 limit cycles can exist only if α is in certain ranges.

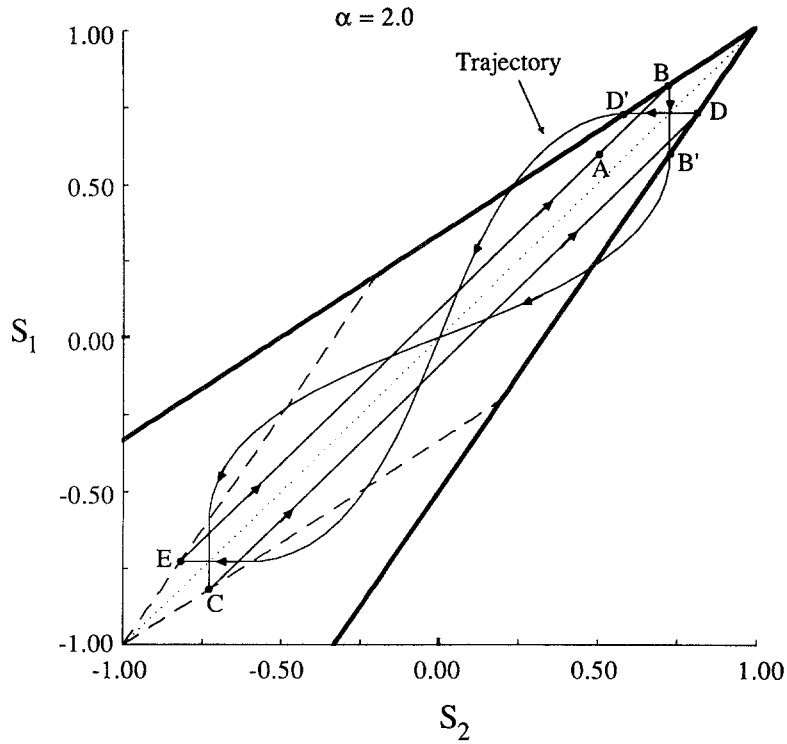

Figure 12

Period-2 Limit Cycle. An alternating asymmetric global event. An initial configuration arbitrarily close to the origin will converge to this period-2 limit cycle (B-B′-C-D-D′-E). The iteration map corresponding to this coupling ratio is shown in the inner square of Figure 8c.

Summary of Model Results

All motions settle to period orbits. The following kinds of periodic motion cycles have been observed, and are illustrated schematically in Figure 13, where the horizontal lines indicate slip, and shading indicates the loading separating events. All periodic motions (one-block *and* two-block events) were found to involve only

single slips of each block. Multislip events were never periodic, but were part of trajectories that settled to periodic orbits.

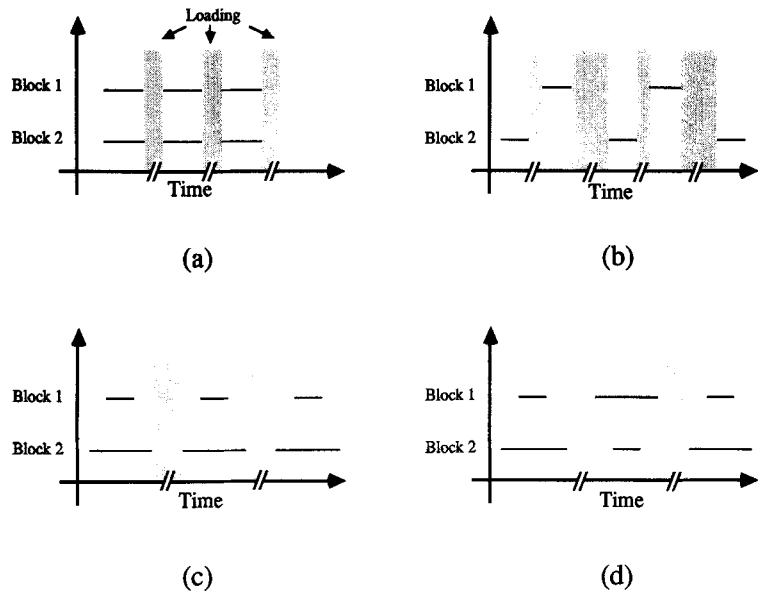

Figure 13

Schematic Figure of Periodic Event Cycles. Horizontal lines indicate times when the given block moves, and shading indicates the loading period between events. As indicated by the breaks in the time axis, the loading period is not shown to scale. In fact, it is much longer than the length of any event. a) Homogeneous event. b) One-block event. c) Nonalternating asymmetric global events. d) Alternating asymmetric global events.

a) Homogeneous events — Only for special values of the spring coupling ratio, $\alpha = (n^2 - 1)/2$ ($n = 2, 3 \ldots$) and a sufficiently homogeneous initial configuration does the system asymptotically approach homogeneous slip. This is *stress smoothing* (in the sense of Andrews). In the exceptional cases when it occurs, the approach to homogeneous slip is very slow.
b) One-block events — For any value of the coupling ratio α, certain ranges of initial configurations result in period-2 orbits. Each event involves slip of a single block. No smoothing is observed. Because of the structural instability of this solution, it is possible that this type of event could drastically change or vanish if the model was slightly changed. However, we have shown that several other friction laws (including one that contained a radiation-simulating linear viscous term) would yield such solutions.
c) Nonalternating asymmetric global events — Some coupling ratios (α)

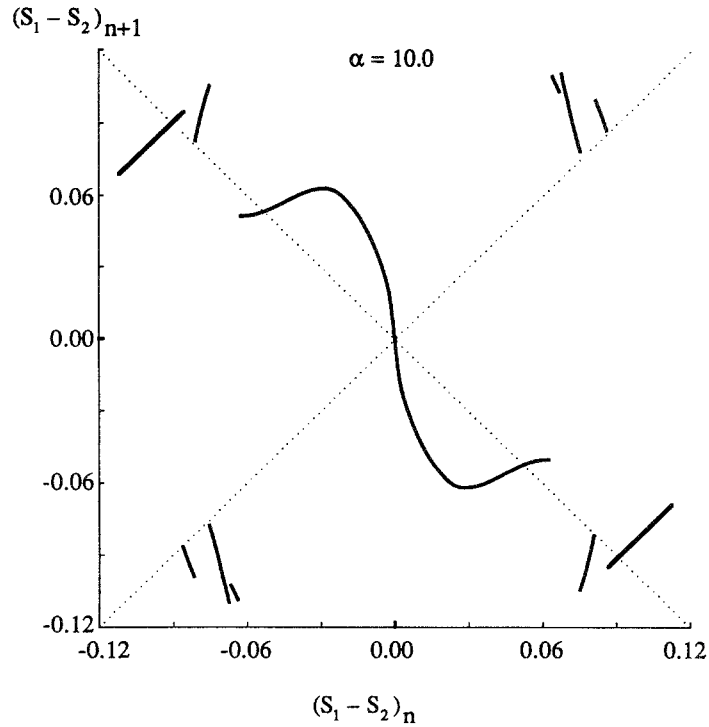

Figure 14

Iteration Map for High Block Coupling. The iteration mapping is more complicated for higher block coupling. Due to the singular nature of static/dynamic friction, high block coupling does not approach a single-block system.

above about 1.3 permit nonalternating asymmetric global-event limit cycles with period 1. The block that slipped first will slip first on the next event.

d) Alternating asymmetric global events — For other values of the coupling ratio above about 1.3, there are stable limit cycles of period 2. The first block to start in one event is the second to start on the following event.

The approach to the limit cycles in (c) or (d) represents *event smoothing* (in the sense of Cao and Aki), but not *stress smoothing*, because the limit cycle configuration is not homogeneous. When these limit cycles exist, certain initial conditions are attracted into them, and others to the period-2 orbits in (b).

Some of these effects depend on the particular choice of friction law. However, the always-observed family of period-2 orbits of (b) will still exist in any model using a slip-displacement or rate dependent friction law. Any friction law with explicit time, absolute position, or state dependence will likely change the shape of Region I, eliminating the family of period-2 one-block orbits. More complex orbits are con-

ceivable, since an appropriate infinitesimal change of the shape of the iteration map graph in Region I (which generates these orbits) can yield arbitrarily complex orbits.

One might expect that for the limit of high coupling, $\alpha \to \infty$, the motion of this two block system should approach that of a single block system. However, such is not observed because of the singular nature of the static/dynamic friction law being used. The iteration map graph for $\alpha = 10.0$ is shown in Figure 14. As is apparent (say from the scales of the iteration map graphs in this paper), the stretch difference $(s_1 - s_2)$ does in fact go to zero for $\alpha \to \infty$. However, the friction force difference during loading, $(1 + \alpha)(s_1 - s_2)$, which is perhaps a more appropriate measure of heterogeneity, remains of order one. It seems clear then that the continuum limit, when the number of blocks is unbounded and α approaches infinity, is not trivial when using the static/dynamic friction law.

Conclusions

In this simple model, perhaps the simplest possible mechanical model for seismicity patterns, we find spatial structure in the 'earthquake' event patterns that is not connected with any spatial structure in the model. Further, all stable solutions break the symmetry of the model (unless special values of the coupling parameters α are chosen). Homogeneous fault stress is generally unstable.

The ultimate slip pattern depends on α, and also on the initial conditions for some values of α. In all cases, one of the following inhomogeneous slip patterns repeats indefinitely:

a) One-block event motions from above which roughly correspond to earthquakes occurring in alternate locations. There is a family of this type of motions, so the relative time between events is indeterminate, and can be close to zero.
b) Nonalternating asymmetric global events which correspond to a repeated earthquake. The location of the epicenter (the first block to move) could be at either block, but remains at that block for all cycles.
c) Alternating asymmetric global events which correspond to earthquakes where the location of the epicenter alternates (between blocks).

Seismicity patterns are generated in this model through dynamics, not through any spatial structure in the model. For any coupling ratio α, there exist initial conditions for which neither stress smoothing nor event smoothing occur. For most values of α, stress smoothing does not occur. That is, the slip difference (or prestress, or self energy) does not go to zero with successive events. The structural instability of some of our solutions implies a great sensitivity to details of the system properties and external loads, and may be related to the complexity of seismic

patterns. It remains to be seen how the results will generalize to more complex and/or asymmetric models.

Acknowledgements

Thank you to Frank Horowitz for computer assistance, and to Mitchell Feigenbaum for an informative public lecture on one-dimensional maps. A discussion with Richard Rand triggered investigation of this particular model. Herbert Hui, Joseph Burns, Joseph Andrews, Jim Papadouplos, Richard Rand, and an anonymous reviewer offered helpful editorial comments. This research was funded by the National Science Foundation and the U.S. Geological Survey, Department of the Interior.

References

ANDREWS, D. (1975), *From antimoment to moment: Plane-strain models of earthquakes that stop.* Bull. Seis. Soc. Am. *65*, 163–182.

ANDREWS, D. (1978), *Coupling of energy between tectonic processes and earthquakes.* J. Geophys. Res. *83*, 2259–2264.

BLANPIED, M. and TULLIS, T. (1986), *The Stability and Behavior of a frictional system with a two state variable constitutive law.* PAGEOPH *124*, 415–444.

BURRIDGE, R. and KNOPOFF, L. (1967), *Model and theoretical seismicity.* Bull. Seis. Soc. Am. *57*, 341–371.

BYERLEE, J. (1970), *The Mechanics of Stick-slip.* Tectonophysics *9*, 475–486.

BYERLEE, J. (1978), *Friction of rocks.* PAGEOPH *116*, 616–626.

CAO, T. and AKI, K. (1984), *Seismicity simulation with a mass-spring model and a displacement hardening-softening friction law.* PAGEOPH *122*, 10–23.

CAO, T. and AKI, K. (1986), *Seismicity simulation with a rate and state dependment friction law.* PAGEOPH *124*, 487–513.

COHEN, S. (1977), *Computer simulation of earthquakes.* J. Geophys. Res. *82*, 3781–3796.

DEVANEY, R. *An Introduction to Chaotic Dynamical Systems* (Benjamin/Cummings Publishing Company, Menlo Part, 1986).

DIETERICH, J. (1972), *Time-dependent friction as a possible mechanism for aftershocks.* J. Geophys. Res. *77*, 3771–3781.

DIETERICH, J., *Experimental and model study of fault constitutive properties.* In *Solid Earth Geophysics and Geotechnology* (ed. Nemet-Nasser) (ASME, NY. 1980) pp. 21–30.

DIETERICH, J. *Constitutive properties of faults with simulated gouge.* In *Mechanical Behavior of Crystal Rocks* (ed. Carter, N. *et al.*) (Geophys. Monogr. *24*, AGU, Washington, D.C. 1981) pp. 103–120.

GU, J., RICE, J., RUINA, A. and TSE, S. (1984), *Slip motion and stability of a single degree of freedom elastic system with rate and state dependent friction.* J. Mech. Phys. Solids *32*, 167–196.

GUCKENHEIMER, J. and HOLMES, P. *Nonlinear Oscillations, Dynamical Systems, and Bifurcations of Vector Fields* (Springer-Verlag, New York, 1983).

HOROWITZ, F. and RUINA, A. (1987), *Frictional slip patterns in a spatially homogeneous elastic fault model*, in revision for J. Geophys. Res.

ISRAEL, M. and NUR, A. (1979), *A Complete solution of a one-dimensional propagating fault with nonuniform stress and strength.* J. Geophys. Res. *85*, 2223–2233.

NUR, A. (1978), *Nonuniform friction as a physical basis for earthquake mechanics.* PAGEOPH *116*, 964–991.

RICE, J. and TSE, S. (1986), *Dynamic motion of a single degree of freedom system following a rate and state dependent friction law*. J. Geophys. Res. *91*, 521–530.

RUINA, A. (1983), *Slip instability and state variable friction laws*. J. Geophys. Res. *88*, 10359–10370.

WEEKS, J. and TULLIS, T. (1985), *Frictional sliding of dolomite: A variation in constitutive behavior*. J. Geophys. Res. *90*, 7821–7826.

(Received August 24, 1986, revised/accepted October 31, 1986)